Experimental Realization of a Three-Dimensional Dirac Semimetal

Sergey Borisenko,[1] Quinn Gibson,[2] Danil Evtushinsky,[1] Volodymyr Zabolotnyy,[1,*] Bernd Büchner,[1,3] and Robert J. Cava[2]
[1]*Institute for Solid State Research, IFW Dresden, P.O. Box 270116, D-01171 Dresden, Germany*
[2]*Department of Chemistry, Princeton University, Princeton, New Jersey 08544, USA*
[3]*Institut fur Festkörperphysik, Technische Universität Dresden, D-01171 Dresden, Germany*
(Received 3 February 2014; published 8 July 2014)

We report the direct observation of the three-dimensional (3D) Dirac semimetal phase in cadmium arsenide (Cd_3As_2) by means of angle-resolved photoemission spectroscopy. We identify two momentum regions where electronic states that strongly disperse in all directions form narrow conelike structures, and thus prove the existence of the long sought 3D Dirac points. This electronic structure naturally explains why Cd_3As_2 has one of the highest known bulk electron mobilities. This realization of a 3D Dirac semimetal in Cd_3As_2 not only opens a direct path to a wide spectrum of applications, but also offers a robust platform for engineering topologically nontrivial phases including Weyl semimetals and quantum spin Hall systems.

DOI: 10.1103/PhysRevLett.113.027603 PACS numbers: 71.55.Ak, 73.22.Pr, 78.40.Kc, 79.60.-i

Semimetals belong to a "buffer zone" between semiconductors and metals and are characterized by a small energy overlap between the conduction and valence bands. This overlap is vaguely defined, partly because the notion of momentum is traditionally not included in the simple classification. In contrast, a three-dimensional (3D) Dirac semimetal, which has been predicted theoretically [1], is precisely defined in terms of the momentum dependent band structure: the mentioned overlap occurs only at a set of isolated points in momentum space where linear energy versus wave vector dispersions cross at the Fermi level. It can be viewed as a 3D generalization of graphene, but in contrast to graphene [2], the Dirac points of such a semimetal are not gapped by the spin-orbit interaction and the crossing of the linear dispersions is protected by crystal symmetry [1]. Such an anomalous Fermi surface in three dimensions would obviously be a source of intriguing physical properties, as is the case with its 2D analog—graphene. Considering a 3D Dirac point as an overlapping of two Weyl points [1,3–5] immediately promotes 3D Dirac semimetals to one of the most wanted new materials from a theoretical point of view: they can be both natively topologically nontrivial and viewed as parent materials for accessing the Weyl semimetal state [6]. In addition to Cd_3As_2, described here, Na_3Bi is another candidate for such a material [5,7].

In order to identify a 3D Dirac semimetal experimentally, one needs to locate a Dirac point in a 3D momentum space and measure the corresponding dispersions of the electronic states. Angle-resolved photoemission spectroscopy (ARPES) is an ideal tool for such a search, and we apply the sub-Kelvin ultrahigh resolution version of this method in the present work (see Ref. [8] and the Supplemental Material [9]). Single crystals of Cd_3As_2 were grown from a Cd rich melt of composition $Cd_{0.85}As_{0.15}$ (see the Supplemental Material [9]). Cd_3As_2 crystallizes in a distorted relative of the antifluorite structure, with Cd in tetrahedral coordination and ordered Cd vacancies [10–12]. A primitive tetragonal crystal structure used for the band structure calculations (see the Supplemental Material [9] and Refs. [10,13]) captures the main features of the electronic structure of cadmium arsenide, including the existence of a single pair of 3D Dirac points along the Γ-Z direction in the BZ (Fig. 1). The theoretical study of Wang *et al.* [14] also shows these 3D Dirac points in Cd_3As_2.

In Figs. 1(a) and 1(b) we compare the results of these relativistic band structure calculations with the data from the ARPES experiment. The typical experimental data set shown represents the valence band of Cd_3As_2. The main dispersion features as well as the bandwidth of 4.5 eV are in good correspondence with the calculations. The discrepancies are due to the inequivalence of the probed and calculated directions in the k space since the actual cleavage plane is (112) [10], and data are thus taken not exactly along the high-symmetry M-Γ-M line. It is also seen that the ARPES signal is effectively defined by a still smaller crystallographic parent subcell of Cd_3As_2—a usual situation when the modulating potential of a lattice distortion leading to a supercell is not very strong and the parent structure is still dominant [15]. This is exactly the case here, as the true unit cell can be viewed as a $2 \times 2 \times 4$ supercell of the parent structure subcell shown in Fig. 1(c), or as a $\sqrt{2} \times \sqrt{2} \times 2$ supercell of the primitive tetragonal unit cell used in the calculations [inset to Fig. 1(c)].

In the region between 0.5 eV and the Fermi level, in agreement with calculations, the photoemission intensity is rather weak; only close to the Γpoint is there a significant amount of intensity, as is expected in the case of strong dispersion along k_z; this is because ARPES is not a bulk sensitive technique and its resolution along k_z is defined by

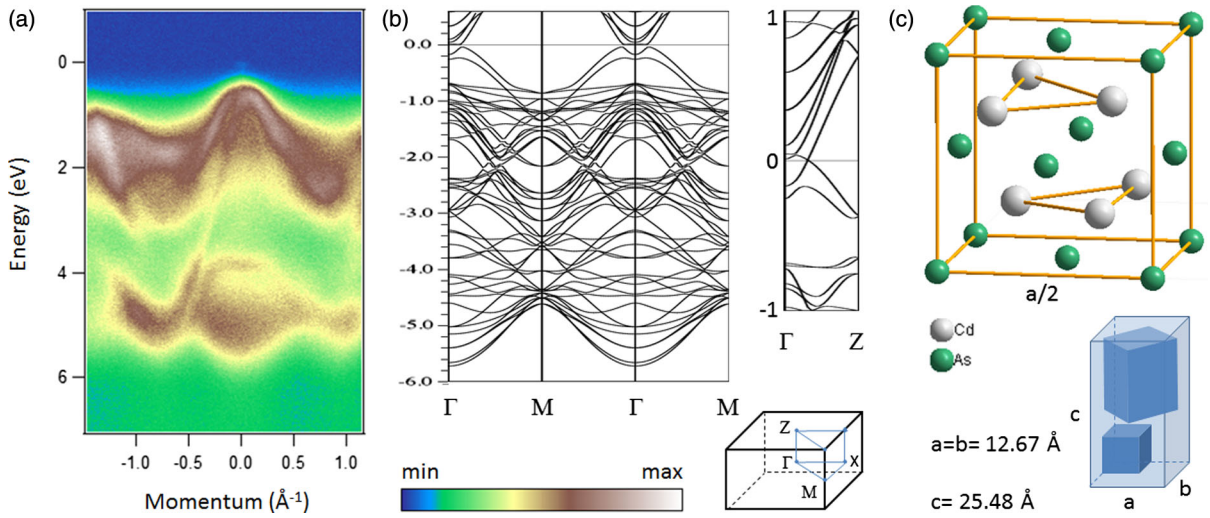

FIG. 1 (color online). (a) Photoemission intensity recorded close to the Γ-M direction using 90 eV photons. (b) Band structure calculations of Cd_3As_2 and its tetragonal BZ. (c) Parent unit cell (with random Cd vacancies). Inset illustrates the relation between the parent, the real one and the one used in the calculations, unit cells.

the escape depth. Nevertheless, we clearly observed the k_z dispersion of the top of the valence band (see Supplemental Material [9]) by approximately 0.25 eV, as predicted by the calculations. Upon closer inspection of the data, one can notice a weak signal connecting the apparent top of the valence band and the Fermi level. In order to find out whether this can be a signature of the sought connection to the conduction band, a scan of the excitation photon energy is required.

We found the suitable experimental conditions to enhance the intensity in the aforementioned region close to the Fermi level. These are the precise angular position of the sample corresponding to normal emission and a particular set of photon energies. One of such data sets taken using $h\nu = 90$ eV is presented in Fig. 2(a). It clearly demonstrates the presence of strongly dispersing electronic states in the 200 meV energy window below the Fermi level. Corresponding to the white arrows in Fig. 2(a), energy- and momentum-distribution curves (EDC and MDC, respectively) are shown in Fig. 2(e). They reveal a well-defined structure that is strongly localized in momentum. In order to resolve the possible fine structure in this region, we have carried out the measurements with the highest possible (at 18 eV photon energy) resolution (~3 meV) at ~0.9 K. The result is shown in Fig. 2(b). We have observed the conelike structure, but without the single dispersions that cross each other as in the case of the surface states of topological insulators [16,17]. This can be considered as a first indication of the presence of a 3D Dirac point, as one expects to see exactly such an intensity distribution in ARPES when k_z can only be defined with significantly worse resolution than the in-plane components. A typical example of this is the bulk conduction band in Bi_2Se_3 [16,17], but here there is a qualitative difference. The dispersions of both conduction and valence bands in Bi_2Se_3 can be tracked more easily since there is a considerable gap between them; the gap results in flat regions in all momenta directions including k_z, thus making them more accessible by ARPES.

We further characterized the narrow conelike electronic feature in other directions of momentum and in energy. Figure 2(c) shows the Fermi surface map with its underlying momentum-energy cuts [right panels of Fig. 2(c)]. As is seen from the map, the feature is also strongly localized along the k_x direction, giving rise to a pointlike Fermi surface. In order to find the energy of the possible touching of the valence and conduction bands we plot the width of the MDCs, as is shown in Fig. 2(e), as a function of binding energy and present the results in Fig. 2(d). Although the curve shows a pronounced minimum at ~75 meV from the Fermi level [Fig. 2(e)], purely visual inspection of the data indicates that the bands touch below 100 meV. Taking into account that the dispersions above and below the Dirac point have different effective masses and the EDC [Fig. 2(e)] has its minimum at ~150 meV, we ascribe this energy to the crossing point of the 3D Dirac cone. The broadening of the MDCs towards the Fermi level clearly implies that the discussed feature is due to the conduction band. The strong in-plane localization of a few hundredths of the BZ size seen in Fig. 2 together with the energy scale of the minimum in the MDC's width are consistent with a very steep dispersion of the conduction band and thus with the absence of the energy gap. This is in very close agreement with the band structure calculations, which show that the crossing is protected by crystal symmetry. From the calculation the conduction band and valence band have different eigenvalues under the $C4$ rotation, so that if they overlap, they can uncross everywhere except where there is $C4$ symmetry (which is everywhere along Γ-Z).

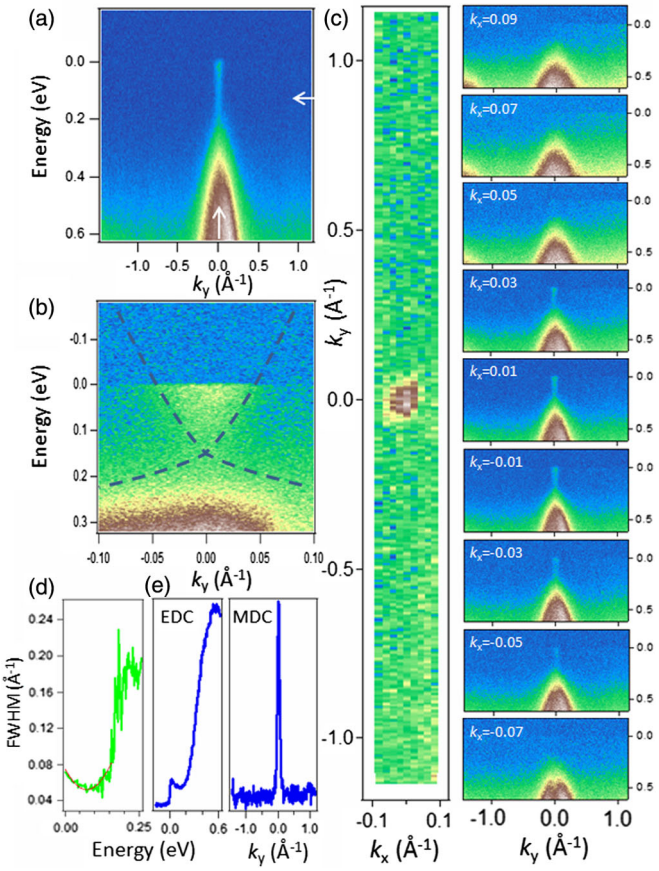

FIG. 2 (color online). (a) Data at 90 eV along the cut going precisely through one of the $k_x = k_y = 0$ points. (b) The same data set taken using the 18 eV photons. Dashed lines are guides to the eye going very close to one of the constant intensity profiles. (c) Fermi surface map (25 meV energy window at the Fermi level) and corresponding intensity plots for each of the k_x momenta. (d) Full width at half maximum as function of energy for the data from panel (b) Red solid line is a fit to the part of the curve. (e) Typical EDC and MDC from (a).

To identify the k_z location of the crossing we have scanned the photon energy in the range from 15 to 110 eV, covering many reciprocal lattice constants in that direction (112). Figure 3 summarizes these results. We observed the narrow conelike electronic feature at only six photon energies in this interval (18, 25, 27, 35, 90, 100 eV). A detailed search found many cases where there was no ARPES intensity connecting the top of the valence band with the Fermi level; we show several of these data sets in Figs. 3(a) and 3(c). This is in sharp contrast with the ARPES intensities observed for surface states, e.g., for topological insulators, where the states are seen with the same clarity essentially independently of the photon energy, unless they are suppressed by matrix element effects. We have used the free electron approximation to calculate the k_z values from the photon energies given in Fig. 3. Using this procedure, there is no value for the inner potential, the only variable parameter in the calculation, which allows one to attribute all the photon energies where the feature is observed to a single k_z value, i.e., solely to the Γ or Z points. Therefore, the Dirac point cannot be at these special wave vectors—it must be located on the line between Γ and Z. From these analyses we conclude that the detected crossing of the valence and conduction bands is of bulk origin, and that it is localized between the Γ and Z points, somewhat closer to the former (see the Supplemental Material [9]). This is in close agreement with the band structure calculations.

The experimental results presented in Figs. 1–3 are consistent with the presence of a single pair of 3D Dirac points in cadmium arsenide, which can thus be considered as the first real material realization of a 3D Dirac semimetal [Fig. 4(a)]. We stress here again that our results are not consistent with the presence of an energy gap. Apart from the reasons mentioned above, as shown in Ref. [14], the gapped material would be a topological insulator and the corresponding surface states would be easily detected in our experiments. The presence of the finite n doping in the current samples slightly shifts the Fermi level from the Dirac points—in analogy to what is often seen with topological insulators [16]. In order to visualize the effect of doping on the electronic structure of the 3D Dirac semimetal, in Figs. 4(b) and 4(d) we show schematically the dispersions and Fermi surfaces for the n- and p-doped cases. An alternative way to depict a 3D Dirac point, in essence a four-dimensional object, is given in Fig. 4(c). Here the energy is represented by the linear color scale, which allows one to restore $E(k)$ curves along an arbitrary direction in the vicinity of the 3D Dirac point. Future materials development or gating experiments are expected to bring the chemical potential down to exactly the Dirac point.

Another similarity of the current compound with known topological insulators is that Cd_3As_2 itself has been known since long ago [18], as were Bi-Sb alloys and Bi_2X_3 thermoelectrics. Earlier studies already indicated that this material is very unusual. Previous interest in Cd_3As_2 has been due to its very high electron mobility [19,20] and its overall electronic properties, which have been attributed to the presence of an inverted band structure [21,22]. Our results are fully consistent with previous experiments. Indeed, the high electron mobility observed, up to 280 000 $cm^2/V\,s$ [20], which is comparable to that of the freestanding graphene, can be explained by considering the fact that the mobility is directly proportional to the Fermi velocity and inversely proportional to the scattering rate and Fermi momentum. As shown above, the Fermi surface of cadmium arsenide consists of two tiny ellipsoids [Fig. 2(c) and Fig. 4(d)] or almost spheres, which is in agreement with earlier Shubnikov–de Haas oscillation [23] studies. This not only implies a small Fermi momentum ($k_F \sim 0.04$ Å^{-1}), but also a strongly reduced scattering rate,

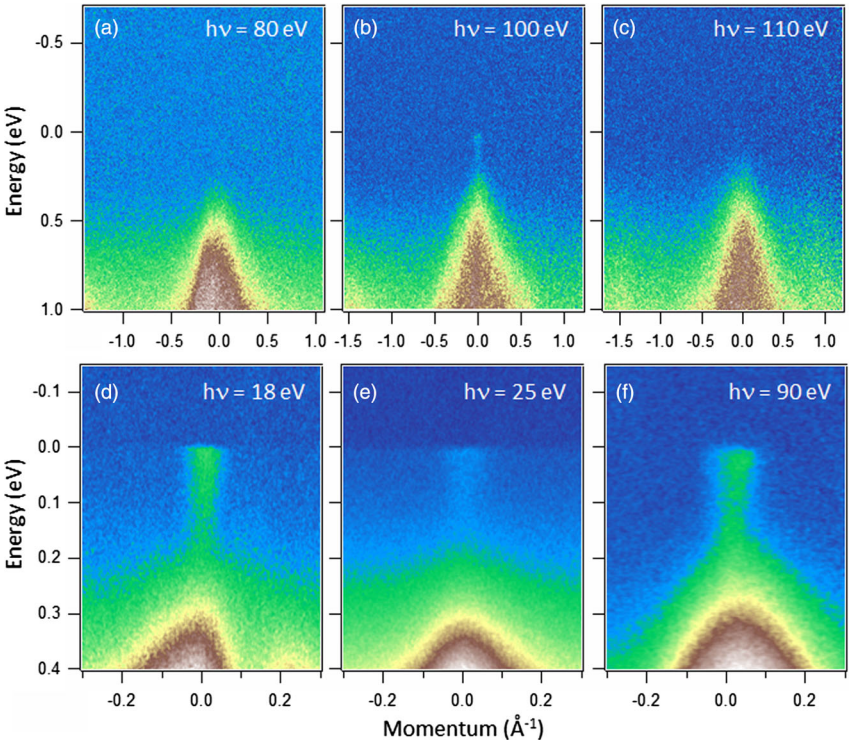

FIG. 3 (color online). ARPES data recorded using different photon energies. In all cases normal emission coincided with the forward direction to the analyzer.

as the phase space for a scattering is extremely small. Knowing the electronic structure from our ARPES data, we can estimate the Fermi velocity. Our estimates from the slopes of the edges of the cones clearly visible in Fig. 3 give the values of 5 ± 2 eV Å, i.e., even higher than those for the usual forms of graphene. All of these factors explain the record high 3D materials' electron mobility in cadmium arsenide.

It has been suggested that a Weyl semimetal can be designed on the basis of a 3D Dirac semimetal by breaking time-reversal or inversion symmetries [3–5]. We cannot at this time speculate whether or not the Weyl state is displayed in Cd_3As_2 as we have not observed any surface states on the (112) cleavage plane. In fact, direct observation of the bulk Dirac points would not be possible, e.g., for the (001) surface because of the overlap with the surface states crossing [5,14]. Wang *et al.* [14] suggest that the 3D Dirac points are degenerate and the Weyl state is not realized; future studies may show this first embodiment of the 3D Dirac semimetal to display the Weyl semimetal state, either in its native state or with the breaking of time reversal symmetry. Cd_3As_2 and the other candidate Dirac semimetal Na_3Bi [5,7] are very different materials from both the conceptual and materials points of view—their symmetries, electronic structures, mobilities, crystal structures, and chemical stability are very different, for example —and thus their detailed comparison in future work will allow for the establishment of the fundamental characteristics of the 3D Dirac semimetal state.

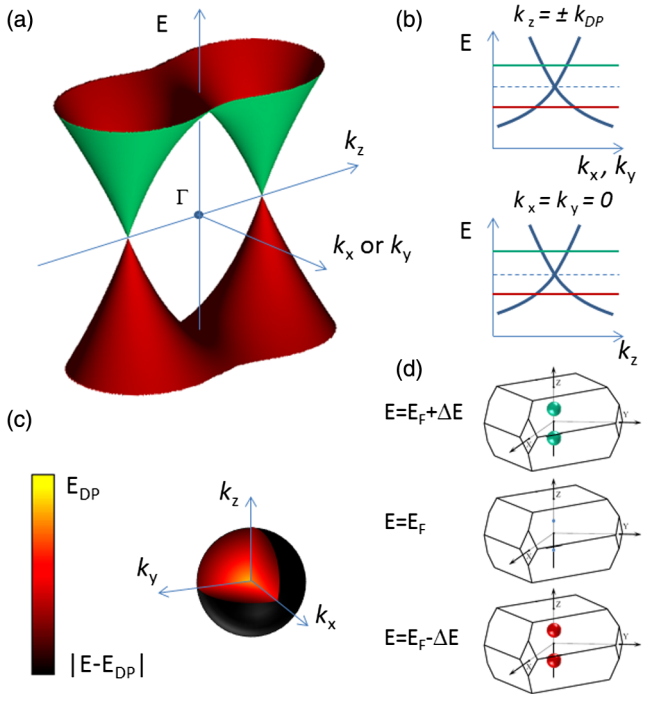

FIG. 4 (color online). (a) Schematic electronic structure of cadmium arsenide. (b) The crossing dispersions along any direction in the momentum space going through the Dirac point. Red (lower) and green (upper) lines correspond to *n*- and *p*-doped cases. (c) An alternative way to depict a 3D Dirac point. (d) 3D Fermi surfaces corresponding to *n*- and *p*-doped (upper and lower panels) as well as undoped cases (middle panel).

The research at Princeton was supported by DARPA-SPAWAR Grant No. N6601-11-4110 and the ARO MURI program, Grant No. W911NF-12-1-0461. R. J. C. thanks the Humboldt Foundation for support. The research in Dresden is supported by Grants No. BO1912/3-1, BO1912/2-2 and No. ZA 654/1-1.

*Present address: Physikalisches Institut, EP IV, Julius-Maximilians-Universität Würzburg, Am Hubland, D-97074 Würzburg, Germany.

[1] S. M. Young, S. Zaheer, J. C. Y. Teo, C. L. Kane, E. J. Mele, and A. M. Rappe, Phys. Rev. Lett. **108**, 140405 (2012).
[2] C. L. Kane and E. J. Mele, Phys. Rev. Lett. **95**, 226801 (2005).
[3] G. B. Halász and L. Balents, Phys. Rev. B **85**, 035103 (2012).
[4] A. A. Burkov and L. Balents, Phys. Rev. Lett. **107**, 127205 (2011).
[5] Z. J. Wang, Y. Sun, X. Q. Chen, C. Franchini, G. Xu, H. M. Weng, X. Dai, and Z. Fang, Phys. Rev. B **85**, 195320 (2012).
[6] X. G. Wan, A. M. Turner, A. Vishwanath, and S. Y. Savrasov, Phys. Rev. B **83**, 205101 (2011).
[7] Z. K. Liu *et al.*, Science **343**, 864 (2014).
[8] S. V. Borisenko, Synchrotron Radiat. News **25**, 6 (2012).
[9] See Supplemental Material at http://link.aps.org/supplemental/10.1103/PhysRevLett.113.027603 for additional data proving the existance of two 3D Dirac points in cadmium arsenide.
[10] Mazhar N. Ali, Q. Gibson, S. Jeon, B. B. Zhou, A. Yazdani, and R. J. Cava, Inorg. Chem. **53**, 4062 (2014).
[11] H. Okamoto, J. Phase Equilib. **13**, 147 (1992).
[12] G. A. Steigmann and J. Goodyear, Acta Crystallogr. Sect. B **24**, 1062 (1968).
[13] J. P. Perdew, K. Burke, and M. Ernzerhof, Phys. Rev. Lett. **77**, 3865 (1996).
[14] Z. Wang, H. Weng, Q. Wu, X. Dai, and Z. Fang, Phys. Rev. B **88**, 125427 (2013).
[15] S. V. Borisenko *et al.* Phys. Rev. Lett. **100**, 196402 (2008).
[16] M. Z. Hasan and C. L. Kane, Rev. Mod. Phys. **82**, 3045 (2010).
[17] A. A. Kordyuk, T. K. Kim, V. B. Zabolotnyy, D. V. Evtushinsky, M. Bauch, C. Hess, B. Büchner, H. Berger, and S. V. Borisenko, Phys. Rev. B **83**, 081303 (2011).
[18] W. Zdanowicz and L. Zdanowicz, Annu. Rev. Mater. Sci. **5**, 301 (1975).
[19] L. Zdanowicz, J. C. Portal, and W. Zdanowicz, Lect. Notes Phys. **177**, 386 (1983).
[20] Arthur J. Rosenberg and Theodore C. Harman, J. Appl. Phys. **30**, 1621 (1959).
[21] Dowgiallo, B. Plenkiewicz, and P. Plenkiewicz, Phys. Status Solidi (b) **94**, K57 (1979).
[22] D. R. Lovett, J. Mater. Sci. **7**, 388 (1972).
[23] I. Rosenman, J. Phys. Chem. Solids **30**, 1385 (1969).